ADVANCED THERAPEUTICS
www.advtherap.com

Controlled Delivery of Paclitaxel via Stable Synthetic Protein Nanoparticles

Ava Mauser, Isabel Waibel, Kaushik Banerjee, Anzar A. Mujeeb, Jingyao Gan, Sophia Lee, William Brown, Nigel Lang, Jason Gregory, Jeffery Raymond, Matthias Franzeb, Anna Schwendeman, Maria G. Castro, and Joerg Lahann**

Despite decades of intense research, glioma remains a disease for which no adequate clinical treatment exists. Given the ongoing therapeutic failures of conventional treatment approaches, nanomedicine may offer alternative options because it can increase the bioavailability of drugs and alter their pharmacokinetics. Here, a new type of synthetic protein nanoparticles (SPNPs) is reported that allow for effective loading and controlled release of the potent cancer drug, paclitaxel (PTX) – a drug that so far has been unsuccessful in glioma treatment due to hydrophobicity, low solubility, and associated delivery challenges. SPNPs are prepared by electrohydrodynamic (EHD) jetting of dilute solutions of PTX-loaded albumin made by high-pressure homogenization. After EHD jetting, PTX SPNPs possess a dry diameter of 165 ± 44 nm, hydrated diameter of 297 ± 102 nm, and a zeta potential of −19 ± 8 mV in water. For the SPNP formulation with a total PTX loading of 9.4%, the loading efficiency is 94%, and controlled release of PTX is observed over two weeks (6% burst release). PTX SPNPs are more potent (68% lethality) than free PTX (45% lethality using 0.2% dimethyl sulfoxide). PTX SPNPs in combination with IR show a significant survival benefit in glioma-bearing mouse models, avoid adverse liver toxicity, and maintain a normal brain architecture. Immunohistochemistry reveals a dramatic tumor size reduction including 40% long-term survivors without discernible signs of tumor. Using flexibly engineered SPNPs, this work outlines an efficient strategy for the delivery of hydrophobic drugs that are otherwise notoriously hard to deliver.

1. Introduction

Glioblastoma IDH wild type (World Health Organization grade 4) is the most common and aggressive form of primary brain cancer with a median survival of ~18 months and has witnessed few therapeutic advancements in the last couple of decades.[1] Challenges that hamper glioblastoma therapeutic efficacy include: i) tumor heterogeneity, ii) treatment resistance, iii) immunosuppressive tumor microenvironment, and iv) difficulties crossing the blood-brain barrier.[1,2] Paclitaxel (PTX) is a promising drug candidate that has had limited clinical success for glioblastoma despite its widespread use for the treatment of breast, lung, ovarian, and Kaposi's sarcoma.[3] Its antitumoral effect is attributed to microtubule stabilization, causing mitotic arrest and inhibiting cell proliferation.[4] Despite the unquestionable potency of PTX, traditional pharmaceutical formulations require solubilization using co-solvents and/or surfactants to improve their bioavailability. Solvent-based delivery of PTX is commonly achieved by solubilization in a mixture of Cremophor EL (CrEL) and ethanol, which are known

A. Mauser, I. Waibel, J. Gan, S. Lee, W. Brown, J. Gregory, J. Raymond, A. Schwendeman, J. Lahann
Biointerfaces Institute
University of Michigan
Ann Arbor, MI 48109, USA
E-mail: lahann@umich.edu

The ORCID identification number(s) for the author(s) of this article can be found under https://doi.org/10.1002/adtp.202400208

DOI: 10.1002/adtp.202400208

A. Mauser, J. Lahann
Department of Biomedical Engineering
University of Michigan
Ann Arbor, MI 48109, USA

I. Waibel, M. Franzeb
Department of Chemical and Process Engineering
Karlsruhe Institute of Technology
76344 Karlsruhe, Germany

K. Banerjee, A. A. Mujeeb, N. Lang, M. G. Castro
Department of Neurosurgery and
Department of Cell and Developmental Biology
University of Michigan Medical School
Ann Arbor, MI 48109, USA
E-mail: mariacas@med.umich.edu

J. Gan, A. Schwendeman
Department of Pharmaceutical Sciences
University of Michigan
Ann Arbor, MI 48109, USA

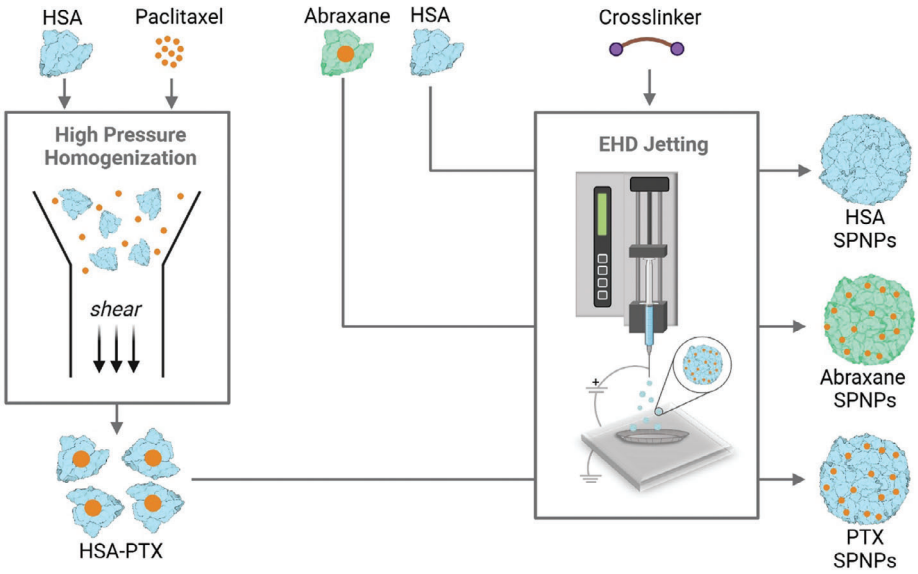

Figure 1. Overview of the preparation of synthetic protein nanoparticles (SPNPs): Human serum albumin (HSA) SPNP (control), PTX SPNP, and Abraxane SPNP. PTX SPNPs were synthesized in a two-step process. First, high-pressure homogenization of HSA and PTX results in protein-bound PTX (HSA-PTX) jetting solutions with well-defined drug content and drug-to-protein ratios. Subsequently, the jetting solutions are processed via EHD jetting to form PTX-loaded nanoparticles (PTX SPNP). For comparison, commercially obtained Abraxane is also processed via EHD jetting, but uses a commercial PTX/albumin formulation as jetting solution. "Empty" nanoparticles without PTX (i.e., HSA SPNP) are also prepared by EHD jetting and are included as a control. Created with BioRender.com.

to cause hypersensitivity reactions[5,6] and hepatic toxicity.[7] Beyond toxicity concerns, CrEL delivery of PTX has non-linear pharmacokinetics due to the intermittent formation of micelles, which entrap PTX and further reduce the amount of free drug available.[8] Therefore, alternative delivery strategies have been explored through the use of nanoparticles such as liposomes, micelles, polymeric nanoparticles, and albumin-bound PTX (e.g., Abraxane).[9] Abraxane is formed through high-pressure homogenization, which uses high shear, cavitation, and pressure; this is referred to more broadly as nanoparticle albumin bound technology. This approach produces physical drug-protein aggregates, where PTX is sequestered within hydrophobic pockets of albumin. However, the resulting aggregates are metastable and rapidly dissociate after administration.[10] Despite stability concerns, Abraxane has witnessed clinical success as it is the first and only FDA-approved protein nanotherapeutic on the market for cancer, including breast cancer, non-small cell lung cancer, and adenocarcinoma of the pancreas.[11] However, low drug concentrations in brain tumors have so far thwarted all therapeutic efforts to use Abraxane, or any other PTX-based therapeutic, for the treatment of glioblastoma, or other gliomas.[12] Abraxane efficacy in brain tumors requires the opening of the blood-brain barrier through low-intensity pulsed ultrasound with microbubble injection.[12] While explored in a clinical trial (NCT04528680), this method requires invasive interventions by implanting a device post-surgical resection to emit ultrasound. Therefore, improvement of the transport of PTX therapeutics to the brain without invasive measures is still needed. If this issue is resolved, it will have major clinical ramifications.

Nanoparticles offer several advantages, such as controlled release, active targeting, and stability, among others. Of the materials available to construct nanoparticles, proteins represent an ideal carrier material due to their versatility, conjugation capabilities, biodegradability, availability and affordability, and relatively low immunogenicity.[13] Recently, chemically stabilized protein nanoparticles have demonstrated effective transport into intracranial brain tumors in mice, resulting in high in vivo efficacy after delivering siRNA and small molecules through fabrication via electrohydrodynamic (EHD) jetting.[14,15] Although these results demonstrate the potential for EHD jetting to produce diverse protein nanomedicines, the current formulations are not optimal to deliver hydrophobic small molecules (such as PTX); largely because the solvent system used to solubilize these drugs are incompatible with the protein nanoparticle requirements. Development of novel processes to prepare nanoparticles equipped with high payloads of hydrophobic drugs is thus critically needed. This is especially so considering that more than 66% of drugs with high potential to treat brain cancer are small molecules,[1] with ≈98% of these drugs cannot access the brain.[16]

Here, we report a versatile platform for the manufacturing of protein nanoparticles containing hydrophobic small-molecule drugs based on EHD jetting of aqueous solvent systems.[17] Our work establishes for the first time that EHD jetting of solutions comprised of protein-bound PTX can result in well-defined and stable protein nanoparticles (**Figure 1**). These systems demonstrate both sustained release profiles of PTX from the nanoparticles and *profound* therapeutic effects in models of glioblastoma.

S. Lee, W. Brown, J. Gregory, J. Raymond, J. Lahann
Department of Chemical Engineering
University of Michigan
Ann Arbor, MI 48109, USA

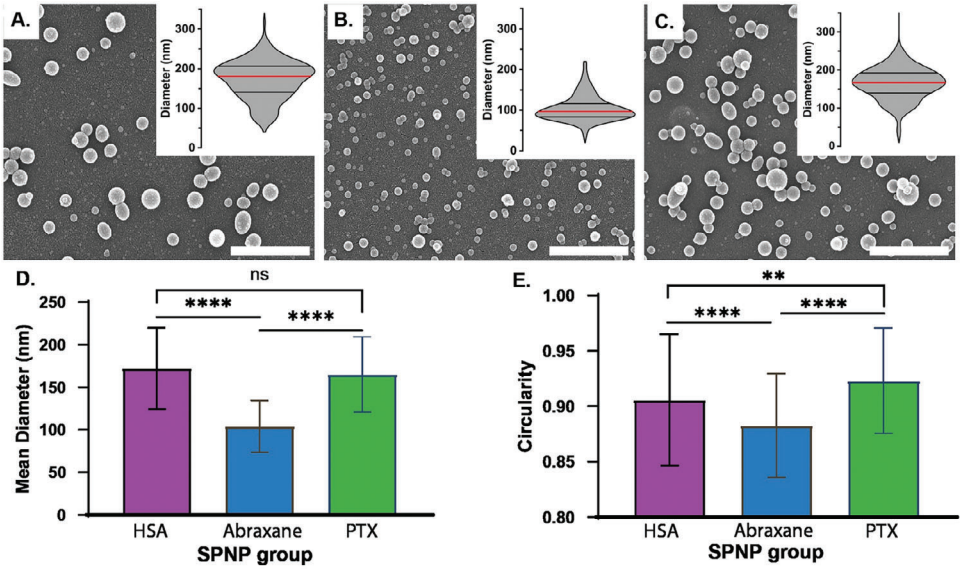

Figure 2. Characterization of as-prepared SPNPs. SEM micrograph images of A) HSA SPNPs, B) Abraxane SPNPs, C) PTX SPNPs (scale bar = 1 µm). The corresponding distributions are shown as insets. Violin plot: pink = median, black = interquartile range. D) Mean diameter from SEM images (HSA SPNP = 173 ± 48 nm, PTX SPNP = 165 ± 44 nm, Abraxane SPNP = 104 ± 30 nm). E) Circularity of HSA SPNPs (0.91 ± 0.06), Abraxane SPNPs (0.88 ± 0.05), and PTX SPNPs (0.92 ± 0.03). ns = not significant, $^{*}p < 0.05$, $^{**}p < 0.01$, $^{****}p < 0.0001$; unpaired t test; $n = 200$.

2. Results and Discussion

As shown in Figure 1, human serum albumin (HSA) synthetic protein nanoparticles (SPNPs) were prepared via electrodhyrdodynamic (EHD) jetting of an aqueous HSA solution (2.5% wt./v). Here, a bifunctional polyethylene glycol (PEG) oligomer was added at 10% wt./wt. relative to HSA to facilitate covalent reactions between amine groups of the HSA and the NHS ester groups, resulting in stable amide bonds. Abraxane SPNPs were produced similarly, but the albumin component was replaced with commercially purchased Abraxane. For the preparation of PTX SPNPs, we used an aqueous jetting solution that was prepared using a lab-scale high-pressure homogenizer (Avestin EmulsiFlex-B15). Briefly, a pre-homogenized crude mixture of PTX (1 mg mL^{-1}) in a saturated chloroform-water mixture was high pressure homogenized at 24 000 psi for 7 cycles, followed by freeze drying.[18] Afterward, the HSA-PTX mixture was aliquoted in ultrapure water. The final jetting solution contained a freshly thawed aliquot of HSA-PTX, ultrapure water, ethylene glycol, and the bifunctional PEG oligomer. The concentrations for all components were matched to the jetting solution used to prepare the HSA SPNPs. In addition, great care was taken to ensure that all EHD jetting parameters were identical for all groups (Table S1, Supporting Information). In brief, the various jetting solutions were mixed, and the jetting solution was loaded into a syringe equipped with a stainless-steel needle and pumped at a rate of 0.1 mL h^{-1}. A positive voltage source was attached to the needle and was grounded to a stainless-steel plate. The voltage was adjusted until a stable Taylor Cone was formed, which occurred between 5 and 8 kV. The charged droplets traveled toward the grounded plate; whereby rapid solvent evaporation produced solid nanoparticles on the grounded collection surface. The solid SPNPs were then stored at 37 °C for 7 days prior to collection in solvent. To assess initial parameters such as size and shape, the dry, as-jetted SPNPs were characterized by scanning electron microscopy (SEM, **Figure** 2A–C).

HSA SPNPs and PTX SPNPs mean diameters were 173 ± 48 nm and 165 ± 44 nm, respectively. The fact that their mean diameters were not statistically different suggests that the jetting solutions must behave very similarly (Figure 2D). In contrast, the average diameter of the Abraxane SPNPs was significantly smaller at 104 ± 30 nm ($p < 0.0001$). The fact that EHD jetting of pressure-homogenized HSA-PTX solutions gave rise to similar particle sizes and polydispersity to those obtained from jetting the drug-free HSA solutions suggests that the payload plays only a subordinary role. The violin plots of each group – shown as an inset of the SEM – indicate very narrow size distributions for all three formulations with PDI values <0.21. We suspect that the lower mean diameter of the Abraxane SPNPs compared to PTX SPNPs is due to residual salt, stemming from the commercially purchased Abraxane. In fact, it is well known that jetting solutions with higher salt concentrations tend to produce nanoparticles with smaller sizes because residual salts increase the conductivity and therefore, decrease the critical droplet size during jetting.[19] Compared to HSA SPNPs, high-pressure homogenization does not alter the sizes and size distributions of the resultant SPNPs after EHD jetting. The size variations are further corroborated by the morphological features of the different SPNP groups. HSA SPNPs (Figure 2A) and PTX SPNPs (Figure 2C) were similar in shape, whereas the Abraxane SPNPs appeared to be more disk-like (Figure 2B). The circularity of HSA SPNPs, PTX SPNPs, and Abraxane SPNPs were 0.91 ± 0.06, 0.92 ± 0.03, and 0.88 ± 0.05, respectively (Figure 2D). A similar trend in the morphological differences can be observed between the SPNPs; the circularity of the Abraxane SPNPs was more significantly different when compared to the PTX SPNPs ($p < 0.0001$) and HSA SPNPs ($p < 0.0001$), whereas the HSA SPNPs and PTX SPNPs are compared with each other ($p < 0.01$).

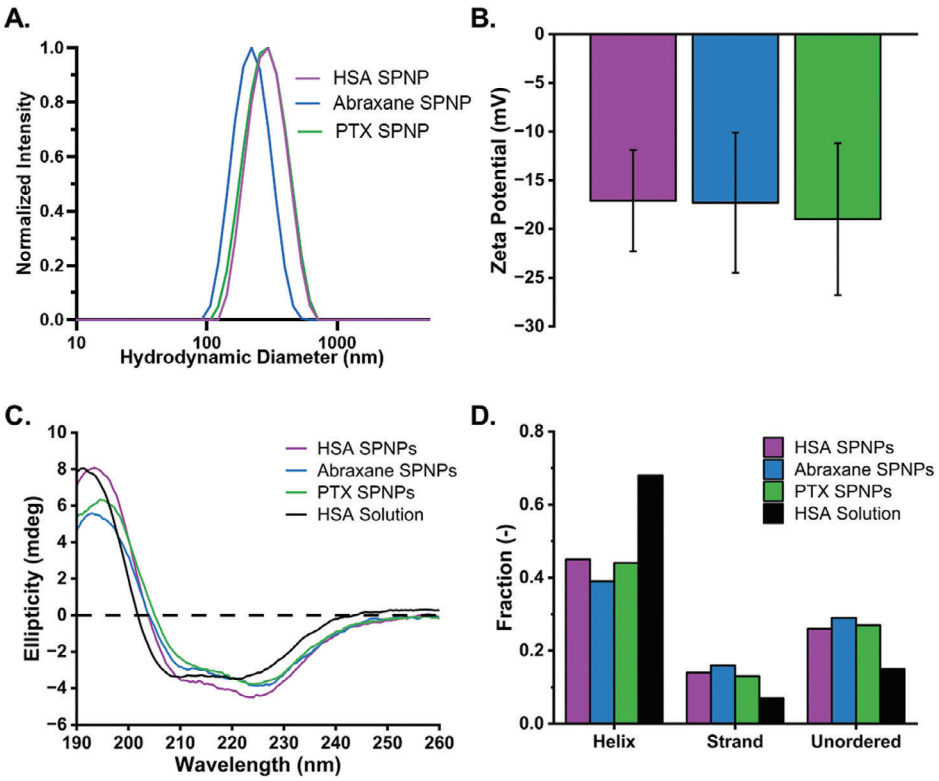

Figure 3. Characterization of HSA SPNPs, Abraxane SPNPs, and PTX SPNPs. A) Intensity-based DLS measured in DPBS. B) Zeta potential in water. C) CD spectra in water. D) Fractions of helix, strand, and unordered secondary structures based on the respective CD spectra determined from Dichroweb analysis.

After EHD jetting, all SPNPs were collected and processed under identical conditions. Briefly, the SPNPs were removed from the collection plate using a dilute surfactant aqueous solution and physical agitation. The collected SPNPs were purified by filtration and serial centrifugation to obtain the final SPNPs. The resulting SPNPs were characterized in water to analyze their hydrodynamic radii, zeta potential, and secondary structure, which was compared to an aqueous solution of HSA (**Figure 3**).

The intensity peak diameter shown in Figure 3A of PTX SPNP, HSA SPNP, and Abraxane SPNP were 297 ± 102 nm, 302 ± 97 nm, and 229 ± 71 nm, respectively. The z-average size was 283 nm for PTX SPNP, 285 nm for HSA SPNP, and 237 nm for Abraxane SPNPs. The PDI for each group was ≈0.30 (PTX SPNP = 0.298, HSA SPNP = 0.305, and Abraxane SPNP = 0.307). The zeta potentials (Figure 3B) were negative for all particle groups (HSA SPNPs = −17 ± 5 mV, Abraxane SPNPs = −17 ± 7 mV, and PTX SPNPs = −19 ± 8 mV) and statistically indistinguishable ($p > 0.05$). The similarity in the DLS spectra shape (unimodal) and the low polydispersity highlight the consistency in the size exclusion methods to obtain the final SPNPs. The incorporation of PTX did not significantly impact nanoparticle size (compared to the HSA SPNPs, which do not contain PTX).

In addition, circular dichroism (CD) spectroscopy was used to assess potential changes in HSA's secondary structure for the various nanoparticle formulations. Figure 3C displays individual CD spectra and compares them to a solution of free HSA. While the spectra of all three SPNP formulations are comparable, they differ from free HSA. A change in CD spectra can indicate a perturbation to the secondary structure of proteins. Here, there is an apparent difference in the spectra from the SNPs and the HSA solution control between 208 and 222 nm. The HSA alpha helix is characterized by two negative bands located at 208 and 222 nm as well as a positive band at 193 nm.[20] To further understand these differences, Dichroweb was used to extract the structural fractions for the helix, strand, and unordered (Figure 3D) secondary domains. The fractions of helix, strand, and unordered for the various SPNPs are similar. We attribute these changes in the protein's secondary structure, in part, to the crosslinking that occurs during the formation of the SPNPs (Figure 3C,D). From Figure S1 (Supporting Information), high-pressure homogenization can alter the secondary structure of HSA and its in accordance with previously published data.[21] We do not expect the EHD jetting itself to impact the protein structure, but rather the chemical reactions of lysine residues of HSA with the bifunctional PEG crosslinker that stabilize the SPNPs. While it is possible that ligand binding or drug binding to HSA can impact the secondary structure of HSA,[22,23] we note the HSA SPNPs without PTX show similar changes in their helical content.

An important aspect of nanoparticle-based delivery systems is their long-term stability. Thus, the stability of PTX SPNPs was assessed by storing the various SPNP formulations in ultrapure water at 4 °C for two weeks (**Figure 4**). In that time course, the secondary structure of the protein was monitored using CD spectroscopy (Figure 4A).

From day 0 to day 14, there were no apparent differences in the CD spectra, indicating that the conformation of the protein

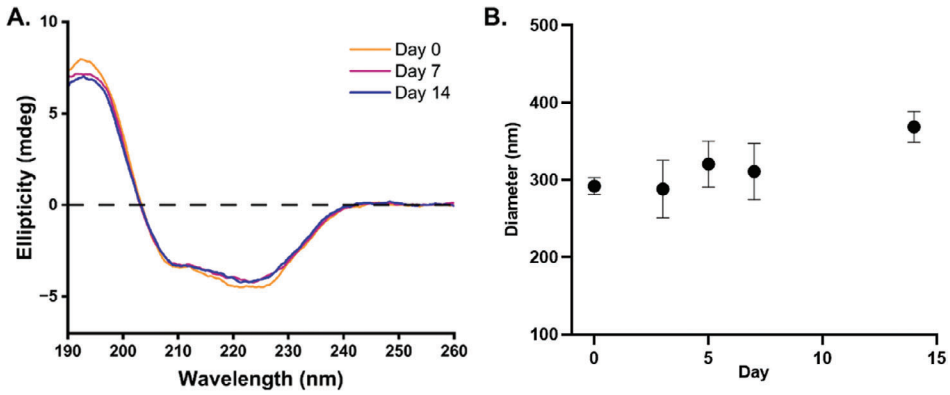

Figure 4. Storage stability of PTX SPNPs in ultrapure water over 14 days. A) CD spectra. B) Intensity peak hydrodynamic diameter. Points are means ($n = 10$) and error bars represent standard deviation.

in the PTX SPNP formulations remained unaltered. In addition, the size of the PTX SPNPs was monitored via DLS. (Figure 4B). The peak size between the first (Day 0) and the last day (Day 14) increased by 76 ± 22 nm, potentially indicating aggregation over time in water. We also examined the long-term storage stability of PTX SPNPs over 143 days in DPBS (Figure S2, Supporting Information). This demonstrates that the SPNPs do trend toward larger sizes when in storage, but aggregation is minimal at even long-term storage (>143 days). Outside of the structural stability, the reproducibility of the PTX SPNPs was examined (Figure S3, Supporting Information). These results show the low run-to-run variability of three batches in Figure S3 (Supporting Information). Each batch was highly circular (circularity > 0.91), as indicated by the SEM micrographs (Figure S3A, Supporting Information). The DLS size distribution was also consistent with spectra overlap between the batches (Figure S3B, Supporting Information) and the zeta potential of the batches did not significantly differ from each other (Figure S3C, Supporting Information).

We next determined the amount of drug loading of PTX in PTX SPNP (Figure S4, Supporting Information). This was accomplished by using a fluorescein isothiocyanate (FITC) labeled PTX (FITC-PTX). FITC-PTX was incorporated into the SPNPs at the same loading as PTX. The absorbance of the FITC-PTX SPNPs was compared to a standard curve of FITC-PTX obtained at a wavelength of 490 nm. Using the equations outlined in the method section, the loading efficiency of PTX in PTX SPNPs was 94% and the total loading of PTX was 9.4%. The use of the FITC-labeled PTX within the SPNPs did not change the size or the morphology of the SPNPs (Figure S4, Supporting Information). Thereafter, we performed a release study to understand the PTX release kinetics from the PTX SPNPs.

In vitro release of PTX from PTX SPNPs was conducted using a dialysis method, whereby PTX SPNPs were placed inside a 10 kDa MWCO membrane dialysis device and allowed to agitate at 37 °C for 2 weeks in release media. The media consisted of distilled water supplemented with 2% (v/v) methanol and 0.1% (v/v) acetic acid relative to methanol. Distilled water was used to avoid artefacts in the UPLC-MS detection. Because PTX has poor water solubility, the media was supplemented with 2% (v/v) methanol. To ensure that the release was not limited by PTX solubility, the methanol concentration was sufficiently high to dissolve three times the total amount of PTX loaded in the PTX SPNPs sample. To avoid transesterification in methanol,[24] which would affect the peak size in UPLC-MS and thus interfere with the quantification of PTX, the media was further supplemented with acetic acid.[24]

We also compared the PTX SPNPs to nanoparticles that were prepared by EHD jetting with jetting solutions that were simple blends of HSA and PTX, that is, they were not subjected to prior high-pressure homogenization. In this case, these non-homogenized PTX SPNPs (nh-PTX SPNPs) were prepared using identical concentrations of HSA, PTX, and crosslinker; however, we used a mixture of 80% (v/v) ultrapure water and 20% (v/v) methanol to ensure solubilization of the PTX. Otherwise, all operational parameters (voltage, distance, flow rate, needle gauge) were identical to those described in Table S1 (Supporting Information). This control group (nh-PTX SPNPs) was fully characterized as summarized in Figure S5 (Supporting Information). We note that the average diameter of these particles was 156 ± 74 nm with a larger PDI of 0.32 (Figure S5, Supporting Information), indicating a higher degree of variability. We used DLS as described above to confirm that the PTX-loaded SPNPs without high-pressure homogenization were stable after EHD jetted (Figure S5, Supporting Information). For both groups (nh-PTX SPNPs and PTX SPNPs), dialysate samples were removed at predetermined time points for subsequent UPLC-MS analysis and PTX quantification (**Figure 5**).

The cumulative PTX release from PTX SPNPs followed a negative amplitude double exponential decay with a half-life ($t_{1/2}$) of 122 h. We observed an initial release regime with a time constant of $\tau_1 = 9.7\ h$, constituting 6% of the total released mass of PTX ($\alpha_1 = 0.06$). The second release regime is characterized by a much longer time constant of $\tau_2 = 302\ h$, constituting 94% ($\alpha_1 = 0.94$) of the total release. The initial fast release can be attributed to the removal of loosely incorporated, near-surface bound PTX, while the second regime is ascribed to the slow release of PTX from the crosslinked HSA matrix of the SPNPs. In contrast, the release profile of the control particles featured a single release regime with a much more rapid rate of release ($\tau = 22\ h$; $\tau_{1/2} = 16.8\ h$), consistent with a fast negative amplitude single exponential decay. For comparison, the half-life of the PTX SPNPs was 122 h, more than seven times longer than that of the control particles. Taken together, high-pressure homogenization prior to EHD jetting has a profound impact on the release kinetics and

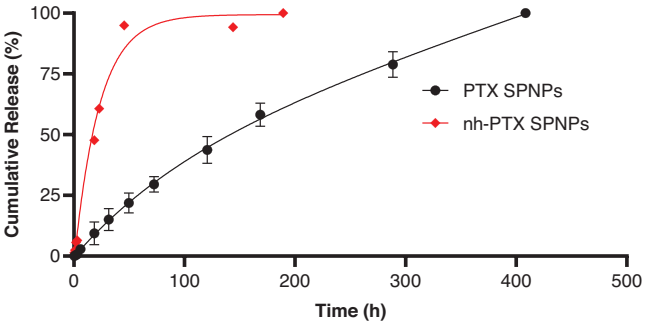

Figure 5. Release profile of PTX SPNPs and nh-PTX SPNPs. The release was conducted at 37 °C in distilled water supplemented with 2% (v/v) methanol and 0.1% ($v/v_{methanol}$) of acetic acid. The release profiles are expressed as % cumulative release relative to the total mass released over the duration of the release. The PTX release from PTX SPNPs followed a double exponential decay shown by the solid black line, whereas the drug release from nh-PTX SPNPs followed a single exponential decay (red solid line). Bars represent mean ± SD ($n = 3$ replicates).

appears to be a prerequisite for the controlled release of PTX from SPNPs.

After characterizing the structure of these PTX SPNPs and validating the use of high-pressure homogenization in the formation of these PTX SPNPs, we next sought to understand their behavior in vitro using two glioma cell cultures. Microtubules play a key role in cellular dynamics, specifically during mitosis. During mitosis, tubulin depolymerization separates chromosomes, which is essential for glioma cell survival and proliferation.[25,26] Microtubule inhibitors like PTX elicit a strong antitumoral effect by stabilizing microtubules, causing mitotic arrest and cell death.[27] Therefore, to assess the activity of PTX SPNPs in vitro, we measured their cytotoxicity in two glioma cell cultures: OL61wtIDH1-EGFRvIII and NPD-AC2wtIDH1-PDGFβ. These genetically engineered glioma cells harbor characteristic genetic alterations encountered in human disease, i,e., EGFRvIII and PDGFβ overexpression. We first sought to establish a dose-response from Abraxane and HSA-PTX formulations to obtain their respective IC_{50} values (Figure S6, Supporting Information). Our results showed that treatment with these solutions markedly inhibited cell proliferation in both glioma cell lines. We determined their IC_{50} values to be 0.42 μM in OL61wtIDH1-EGFRvIII cells and 0.19 μM in NPD-AC2wtIDH1-PDGFβ cells. The observed potency was comparable to Abraxane, which had slightly higher IC_{50} values of 1.84 and 1.45 μM in the OL61wtIDH1-EGFRvIII and NPD-AC2wtIDH1-PDGFβ cells. We next tested the hypothesis that the collected SPNP formulations will have enhanced potency. We thus repeated the cell viability assays with both OL61wtIDH1-EGFRvIII and NPD-AC2wtIDH1-PDGFβ cell cultures using nanoparticle doses informed by the IC_{50} values. Three doses of PTX SPNPs were prepared that corresponded to 0.1-fold (0.1×), onefold (1×), and tenfold (10×) of the IC_{50} value observed for HSA-PTX solutions ("x" denotes the IC_{50} value). These doses were prepared by calculating the amount of SPNPs needed to reach that IC_{50} based on a PTX loading of 9.4%. We compared these groups to the high-pressure HSA-PTX formulations with identical doses and included saline and free PTX (0.2 μM) as additional controls. Our results demonstrated that PTX SPNPs are more potent (32% viability) than HSA-PTX or PTX (55% viability) ($p = 0.0145$) (**Figure 6**). In contrast, HSA SPNPs had no overt toxicity in either glioma cell tested; even at doses equivalent to tenfold the IC_{50} values. For both cell cultures, the PTX SPNPs were more effective than the HSA-PTX formulation. This could be attributed to the difference in stability, because the PTX SPNPs were stabilized via crosslinking as part of the particle fabrication process. HSA-PTX formulations are known to dissociate into albumin-PTX subunits upon administration.[10]

To assess the efficacy of PTX-SPNP in vivo, mice were implanted with NPD glioma cells in the right striatum. Glioblastoma-bearing mice were treated with multiple doses of SPNPs or Abraxane with and without radiation since radiation therapy is the standard of care for glioblastoma. The dosing schedule is shown in **Figure** 7A where Abraxane and SPNPs were administered three times a week for two weeks and radiation was administered five times a week for two weeks.

The results showed that treatment with IR alone (standard of care) or Abraxane did not cause a statistically significant change in the median survival (MS) (Figure 7B). Treatment with the HSA SPNP resulted in a MS of 27 days, which was non-significant compared to the saline control ($p = 0.0825$). Abraxane, in combination with radiation, also resulted in a MS of 27 days (Figure 7C). In contrast, treatment with PTX SPNP alone or in combination with radiation substantially increased the MSto 29 days (Figure 7B) and 37 days (Figure 7C)., respectively (PTX SPNP+IR vs saline (p = 0.0018, **)). Comparing PTX SPNP+IR with HSA SPNP, we found that the increase in survival was also statistically significant [PTX SPNP+IR vs HSA SPNP ($p = 0.0198$, *)]. Glioblastoma-bearing mice that were treated with PTX SPNP in combination with IR resulted in 40% long-term survivors which were tumor free. A full statistical analysis is available in Table S2 (Supporting Information).

In addition, we assessed a panel of biomarkers to evaluate each treatment group's healthy liver and kidney function in the survival study (Figure S7, Supporting Information). Serum levels of Creatinine, BUN, ALT, ALB, AST, ALKP, TPRO, and TBIL did not significantly change for any of the treatments. The levels of different serum biochemical parameters between the treatment groups were non-significant (Figure S7, Supporting Information). In addition, hematoxylin and eosin (H&E) staining of liver sections from different groups revealed no adverse treatment effects on the liver. No notable differences were observed in the histological characteristics of hepatocytes and stromal regions within both central and portal areas between the different groups (Figure S8, Supporting Information).

Microscopic examination showed no evidence of intracranial tumor in long-term survivors (Figure 7D). In contrast, H&E staining revealed the presence of a tumor in the hemisphere region of the saline, IR-treated mice, and the HSA SPNP-treated mice. No apparent areas of hemorrhages, necrosis, or invasion were present in the long-term survivors after receiving the combination therapy, PTX SPNP +IR. To assess whether the combination treatment affected the surrounding brain architecture, we performed immunohistochemistry staining using glial fibrillary acidic protein (GFAP) and myelin basic protein (MBP) as marker for myelin sheath integrity. Results showed no apparent changes in brain architecture in mice receiving the combined PTX SPNP +IR treatment (Figure 7D).

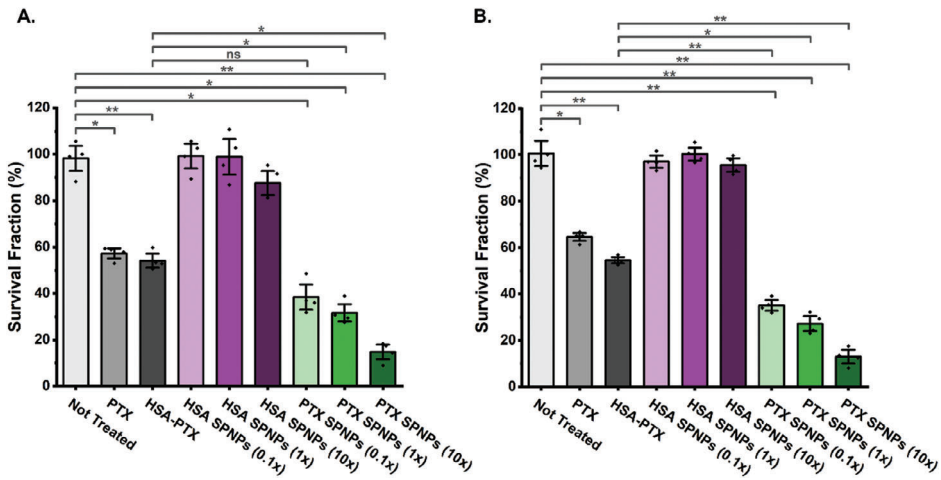

Figure 6. PTX SPNPs display high efficacy in murine glioma cells. OL61 (shp53/NRAS/EGFRvIII) A) and NPD-AC2 (shp53/NRAS/PDGFβ) B). mouse glioma cells were treated with either PTX, HSA-PTX, or with PTX SPNP either at their respective IC_{50} doses on the corresponding mouse glioma cells or at the indicated doses (i.e., 0.1× is 0.1 times the IC_{50} dose of HSA-PTX) for 72 h. The bar plots show the % of viable glioma cells after treatment with saline, free-PTX, free HSA-PTX, PTX, or PTX SPNP. Free PTX and HSA-PTX treatments were done at IC_{50} doses for the corresponding mouse glioma cells. ns = non-significant, $^{*}p < 0.05$ $^{**}p < 0.01$; unpaired t test. Bars represent mean ± SD ($n = 4$ biological replicates).

To assess the level of immune cellular infiltrates, brain tissue sections of mice from the same experimental groups were evaluated by immunohistochemistry using markers for macrophages (CD68) and microglia (IBA1) (Figure S9, Supporting Information). The immunocytochemistry analisis showed increased infiltration of macrophages (CD68+ cells) within the tumor microenvironment and the adjacent brain parenchyma in the group that received either IR or HSA SPNP (Figure S9, Supporting Information). In contrast, the long-term survivors from the PTX SPNP +IR group have a reduced number of CD68+ macrophages compared to the other groups (Figure S9, Supporting Information). The results revealed a noteworthy reduction in tumor size concomitant with a decrease in the presence of CD68-positive cells following the combined treatment. We also observed IBA1+ microglia within the tumor microenvironment and the surrounding brain parenchymain combination in all the groups. Of note, we observed a reduced level of IBA1 expression in PTX SPNP +IR long-term survivors compared to all other treatment groups.

3. Conclusion

Here, we report the production and characterization of stable SPNPs for controlled release of the hydrophobic antineoplastic agent, PTX. These PTX SPNPs were prepared via electrohydrodynamic jetting of HSA-PTX formulations with PTX loadings as high as 9.4%. Through control experiments, we confirmed the controlled release of PTX with minimal burst (6%) and established that high-pressure homogenization prior to electrojetting is a prerequisite for the controlled release of PTX. The differences in nanoparticle formulations resulted in significant improvement in their therapeutic activity against glioma cells. When PTX SPNPs were administered in combination with IR, 40% of the glioblastoma-bearing mice showed long-term survival. More generally, the work constitutes a novel framework to produce precisely engineered protein nanoparticles for the controlled release of hydrophobic drugs via electrohydrodynamic jetting.

4. Experimental Section

Materials: Acetic acid (A6283), HSA (A1653), ethylene glycol (102 466), O,O′-Bis[2-(N-Succinimidyl-succinylamino)ethyl]polyethylene glycol (#713 783), Tween20 (P2287), chloroform (C2432), formic acid (A117), HPLC-grade methanol (34 860), Hellmanex III (Z805939) were purchased from Sigma–Aldrich. Albumin from bovine serum albumin, Alexa Fluor 647 conjugate (A34785), LC-MS grade water (51 140), ProLong Gold antifade reagent (P10144), and LC-MS grade acetonitrile (A955), were purchased from ThermoFisher Scientific. Ultrapure distilled water (10 977) distilled water (15230-162), Dulbecco's modified eagle medium (DMEM) (12430-054), L-Glutamine (11360-070), antibiotic-antimycotic (anti-anti) (15240-062), DMEM with F-12 (11330-032), B-27 (12587-010), N-2 (17502-048) and Dulbecco's Phosphate Buffered Saline (14190-144) were purchased from Gibco. Abraxane (E1068) was purchased from Selleckchem. Pierce 660 nm protein assay reagent (22 660), pre-diluted protein assay standards of bovine serum albumin set (23 208), Pierce BCA protein assay kit (23 225), and dialysis devices (Slide-A-Lyzer MINI Dialysis Devices, 0.5 mL) were purchased from Thermo Scientific. PTX (P-9600) was purchased from LC Laboratories. Fluorescein isothiocyanate (FITC) labeled -PTX (#R-OR-040) was purchased from Ruixibio. CellTiter-Glo 2.0 (#G9242) was purchased from Promega. Anti-CD3ϵ (D4V8L) was purchased from Cell Signaling (#99940S), Anti-CD68 (#ab125212) and Anti-Ibal (#ab178846) were purchased from Abcam. Anti-MBP (#MAB386) and Anti-GFAP (#AB5541) were purchased from Millipore. Fetal bovine serum (FBS) (S1520-500) was purchased from Biowest. Growth factors hFGF (100-18B-1MG) and hEGF (AF-100-15-1MG) were purchased from Peprotech. Normocin (anti-nr-2) was purchased from Invivogen.

Glioma Cell Lines and Culture Condition: Genetically engineered mouse glioma models: OL61 (shp53/NRAS/EGFRvIII) and NPD-AC2 (shp53/NRAS/PDGFβ) were developed by the sleeping beauty transposon system as described before.[28–30] OL61 cells were grown in DMEM supplemented with 10% FBS, 200 mM L-Glutamine (1×), 100 µg mL^{-1} Normocin and 100 units mL^{-1} anti-anti. NPD cells were grown in DMEM nutrient mixture F-12 with L-Glutamine (DMEM/F-12 (Ham) (1:1) (1×); supplemented with 2% 1× B-27, 1% 1× N-2, 100 µg mL^{-1} Normocin and 100 units mL^{-1} antibiotic-antimycotic (Anti-Anti, Gibco, 15240-062). In addition, hFGF and hEGF were supplemented twice weekly at 20 ng mL^{-1}.[31,32]

Fabrication of HSA-PTX: HSA-PTX was produced using high-pressure homogenization.[18] PTX (30 mg) was dissolved in 550 µL of chloroform at 37 °C. Meanwhile, chloroform (5 mL) was added to 37.5 mL of distilled

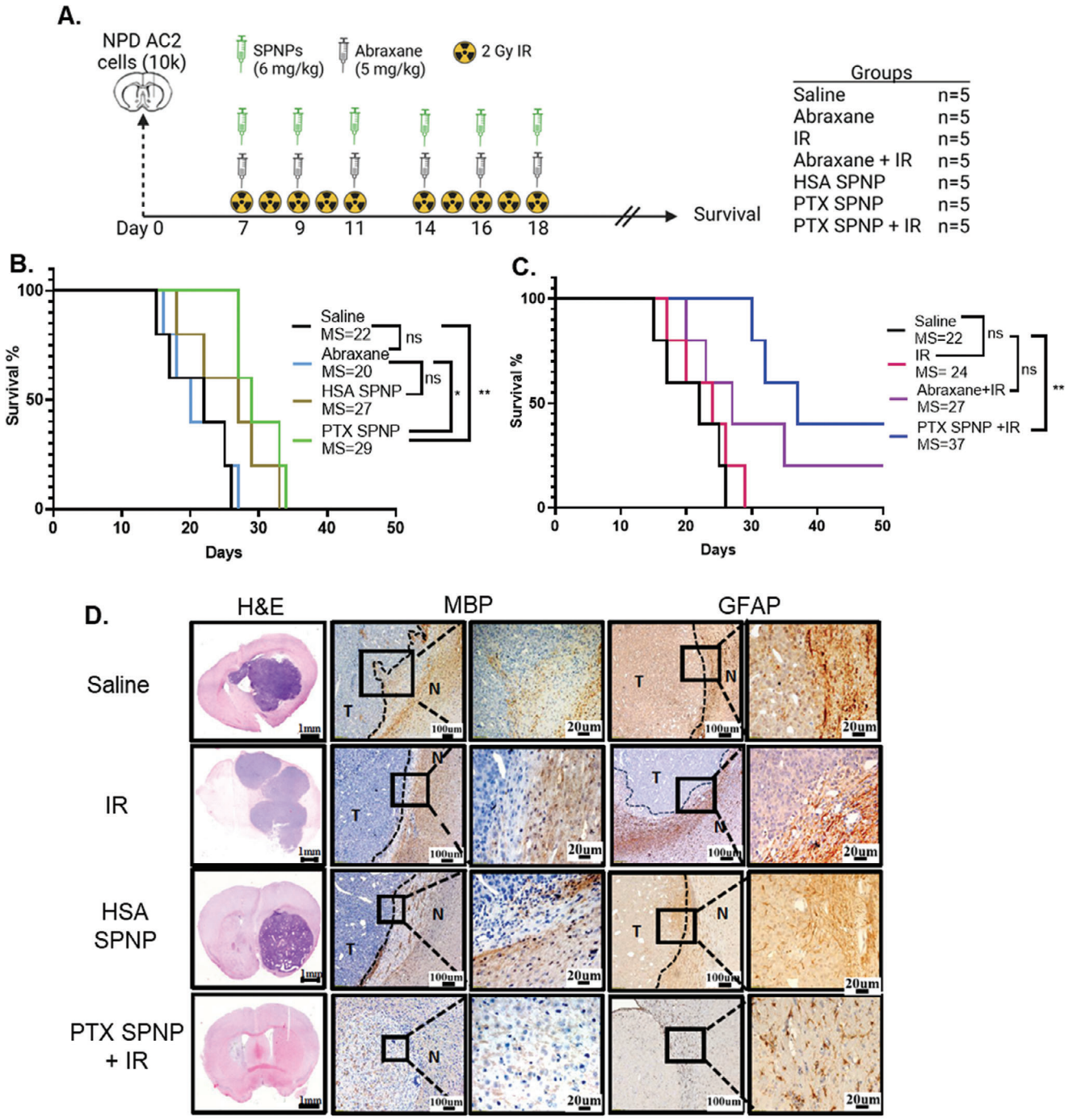

Figure 7. Efficacy of PTX SPNPs in NPD tumor bearing mice. A) Illustration depicting the treatment schedule of SPNPs (PTX SPNP or HSA SPNP) and Abraxane with and without IR. After tumor implantation on day 0, treatment began on day 7 and ended day 18. The groups tested were saline, Abraxane, IR, Abraxane + IR, HSA SPNP, PTX SPNP, and PTX SPNP + IR, each with $n = 5$ mice per group. B) Kaplan-Meier survival curves for groups treated without IR (saline, Abraxane, HSA SPNP, PTX SPNP). C) Kaplan-Meier survival curves IR-treated groups (saline, IR, Abraxane + IR, PTX SPNP + IR). Ns = not signficant, $^{*}p < 0.05$, $^{**}p < 0.01$; log-rank (Mantel-Cox) test. MS= median survival. D) Hematoxylin and eosin (H&E) staining of 5 µm paraffin-embedded brain sections from saline, IR, HSA SPNP, and long-term survivors from PTX SPNP + IR treatment groups (scale bar = 1 mm). Paraffin-embedded 5 µm brain sections for each treatment groups were stained for myeline basic protein (MBP), and glial fibrillary acidic protein (GFAP), Low magnification (10×) panels show normal brain (N) and tumor (T) tissue (black scale bar = 100 µm). High magnification (40×) panels (black scale bar = 20 µm) indicate positive staining for the areas delineated in the low-magnification panels. Representative images from a single experiment consisting of independent biological replicates are displayed.

water and vortexed. The mixture was allowed to settle to produce two phases: chloroform, and water saturated with chloroform. The saturated top phase was removed and 29.4 mL of it was added to 294 mg of HSA. Once the HSA was solubilized, the dissolved PTX solution was added. The crude mixture was then tip-sonicated at an amplitude of 50 for 1 min continuously at room temperature to pre-homogenize the mixture. The pre-homogenized solution was split between two 20 mL syringes for high pressure homogenization with the Avestin EmulsiFlex-B15. The mixture was homogenized for 7 cycles at 24 000 psi. The resulting homogenized sample was then frozen at −20 °C, lyophilized over 72 h, and weighed. Aliquots were prepared by resuspending the homogenized HSA/PTX in ultrapure water at a concentration of 39.33 mg mL^{-1}. To produce FITC-labeled HSA-PTX, FITC-PTX was used instead of the PTX. The amount of FITC-PTX was scaled to have the same contribution of PTX in the crude mixture.

Fabrication of SPNPs: Electrohydrodynamic (EHD) jetting was used to produce nanoparticles as previously described.[14,15,21,33] The distance from the tip of the needle and the collection plate was maintained at 9 cm, with a positive voltage lead attached to the tip of the needle, and a grounding lead connected to the stainless-steel platform beneath the aluminum collection plate. To produce HSA SPNPs, the jetting formulation consisted of 2.5% (wt./v) HSA, which was solubilized in a co-solvent system of 1:4 ethylene glycol to ultrapure water. Next, a bi-functional crosslinker, [O,O'-Bis[2-(N-Succinimidyl-succinylamino)-ethyl]polyethylene glycol], was added at 10% ($wt./wt._{protein}$). The PTX SPNPs and Abraxane SPNPs were formulated similarly, but instead of pure HSA, HSA-PTX, and commercially available Abraxane were used, respectively. The PTX SPNPs prepared for the in vivo study contained iRGD peptide at 8.6 µg per mg of HSA and was added into the formulation prior to the ethylene glycol and crosslinker. The PTX SPNPs without high-pressure homogenization consisted of 2.5% (wt./v) HSA, 10% PTX, and a co-solvent system of 20% (v/v) methanol and 80% (v/v) water. The crosslinker was added at 10% (wt./wt.) relative to the HSA like the other formulations. The jetting solutions were filled into a 1 mL syringe equipped with a 25-gauge stainless steel needle and was pumped at a rate of 0.1 mL h^{-1} onto an aluminum collection plate. The voltage (5–8 kV) was applied to form a stable Taylor Cone. The collection plate was changed every 30 min, then placed into an incubator at 37 °C for 7 days to crosslink.

Collection and Processing of SPNPs: After crosslinking for 7 days at 37 °C, SPNPs were collected following protocols previously described.[15,33] Briefly, 3–5 mL of collection buffer (0.05% v/v Tween20 in DPBS) was added to the crosslinked SPNPs and physically agitated with a plastic razor blade in order to release the nanoparticles from each aluminum collection plate. The solution with released nanoparticles was then transferred to a 50 mL falcon tube, tip sonicated in an ice bath for 30 s at an amplitude of 5 (1 s on, 3 s off), then filtered through a 40 µm cell strainer. The filtered particles were then centrifuged at 3200 rcf for 5 min at 4 °C. The pellet was discarded, and the supernatant was further processed; it was split into 2 mL Eppendorf tubes then centrifuged at 22 300 rcf for 1 h at 4 °C. The supernatant was discarded, and the pellets were combined. The combined pellet was washed with ultrapure water for characterization studies. For in vitro and vivo studies, the pellet was resuspended in DPBS within 6 h prior to use.

Scanning Electron Microscopy (SEM): Scanning electron microscopy (SEM) was performed to characterize nanoparticles in their dry state. For EHD jetted samples, silicon wafers were placed on top of the aluminum collection plate during jetting, then adhered onto an SEM stub equipped with double sided copper tape. All samples were gold sputter coated (50 s), then imaged using the FEI Nova 200 SEM/FIB. The following parameters were used for all imaging: voltage of 17 kV, current of 0.14 nA, and a dwell time of 10 µs.

SEM Analysis: SEM images were analyzed with ImageJ using previously described protocols.[33] Two hundred unique nanoparticles were characterized for each nanoparticle type to obtain an average diameter, circularity, and PDI.

Dynamic Light Scattering (DLS) and Electrophoretic Light Scattering (ELS): Hydrated nanoparticles were characterized using the Zetasizer Nano ZS (Malvern Panalytical) for size and zeta potential measurements. Nanoparticles were diluted to a concentration of 0.0375 mg mL^{-1} in ultrapure water. For stability studies, the same sample was measured at the predetermined time point. New disposable low volume cuvettes were used for each measurement. Stability over 14 days was conducted in ultrapure water and ten individual scans were used to obtain each peak measurement data point. The error bars were expressed in standard deviations. Stability over 143 days was conducted in DPBS.

Nanoparticle Tracking Analysis: Concentration and size distribution of hydrated SPNPs were measured using the Nanosight Nanoparticle Tracking Analysis (NTA) device. Samples were prepared by diluting the SPNPs with ultrapure distilled water by a factor of 800 to a final volume of 1 mL. The sample was loaded into a 1 mL disposable syringe and placed within the syringe pump of the NTA. The measurement was performed a total of five times with a sCMOS camera, a camera level of 9, a 488 nm laser, a syringe pump speed of 20 AU, a temperature of 24 °C, and a capture duration of 60 s. After capture, the videos were analyzed by the built-in NanoSight Software NTA 3.1 Build 3.4.4. with a detection threshold of 7. All videos passed the software's quality check.

Protein Concentration: Protein concentration was determined using the Pierce 660 nm protein assay reagent with pre-diluted protein assay standards (Bovine Serum Albumin) set and the Pierce BCA protein assay kit following the manufacturer's protocol.

Circular Dichroism (CD) Spectroscopy: Circular dichroism (CD) spectroscopy was used to understand how the nanoparticle fabrication method affected the secondary structure of the proteins over time. Measurements were taken in a 1 mm Jasco quartz cuvette via the Jasco J-815 spectrometer in a range of 260–190 nm with a data pitch of 0.2 nm, digital integration time of 1 s, bandwidth of 1.0 nm, scan speed of 100 nm min^{-1}, and total of 3 accumulations per measurement. Between each CD measurement, the cuvette was washed in Hellmanex III cuvette cleaning solution at (2% v/v in DI water) for 5 min at 80 °C then washed ten times with deionized water and finally washed with ethanol to expedite the drying time. Each sample was diluted in ultrapure water to 37.5 ug mL^{-1}. Dichroweb was used to quantify the fraction of each secondary structure using the CDSSTR method with reference set 7.[34–36]

Ultra-Performance Liquid Chromatography – Mass Spectroscopy (UPLC-MS): PTX was weighed and dissolved in 50% (v/v) methanol and 50% (v/v) ultrapure water to produce a series of standard solutions (500, 250, 125, 62.5, and 31.25 ng mL^{-1}). The PTX from in vitro release experiments and from loading experiments were performed using a ACQUITY UPLC H-Class PLUS equipped with a quaternary solvent manager, an FTN-H sample manager, a heated column compartment, a TUV detector and an ESI mass detector (Qda). The chromatographic detection was performed using an ACQUITY UPLC BEH C18 column (2.1 × 50 mm, 1.7 µm, Waters) by isocratic elution with the mobile phase comprised of 0.1% formic acid in water: acetonitrile (60:40%, v/v) at a flow rate of 0.8 mL h^{-1}. An injection volume of 10 µL and a detection wavelength of 227 nm was used. The column and samples were maintained at a temperature of 25 and 4 °C, respectively. The run time was 5 min, and the retention time was 2.4 min. Mass spectral data were obtained in positive electrospray mode (ESI+) in MRM mode for PTX at m/z of 876.44.

In Vitro Release: PTX SPNPs and nh-PTX SPNPs were collected, processed, and characterized as described above. The PTX SPNPs (1000 µg mL^{-1}, 1 mL) were placed inside a 15 mL 10 kDa MWCO dialysis membrane (Slide-a-Lyzer) with the release medium of distilled water with 2% (v/v) methanol and 0.1% (v/v) acetic acid relative to the methanol. The device was allowed to shake continuously at 37 °C for 17 days. At predetermined time points, 2.5 mL of the dialysate was removed and frozen at −20 °C and replaced with 2.5 mL of release medium. The frozen samples were lyophilized overnight, resuspended in 1 mL of 50% v/v methanol in ultrapure water then analyzed via UPLC-MS.

Loading Efficiency: Centrifugal spin filtration and UPLC-MS detection were used to determine the loading efficiency of the HSA-PTX. Lyophilized HSA-PTX was resuspended in ultrapure water at a concentration of 3.28 mg mL^{-1} in a 1:5 methanol:water (v/v) solution. Spin filters (100 and 10 kDa) were prepared according to the manufacturer's instructions. The suspension was split between two prepared 100 kDa spin filters (300 µL each) and spun down at 5000 rcf for 1 min. The filtrate was removed, and the filter was replenished with additional suspension solvent

(1:5 methanol:water, (v/v)) at 5000 rcf and 10 000 rcf for the second, and third time, respectively, for 1 min each spin. For the 4–10 subsequent washes, the speed remained constant at 15 000 rcf for 1 min. After processing with the 100 kDa filter to separate any unbound HSA and PTX, the dialysate from the first filtration was subjected to an additional filtration step. The filtrate (HSA and PTX) was added to 10 kDa spin filters and washed with the methanol/water mixture for ten times at 15 000 rcf for 1 min each wash. The filtrate from the second filtration step was analyzed via UPLC-MS to determine unbound or unloaded PTX in the HSA-PTX. The following equation was used to calculate the loading efficiency based on mass.

$$Loading\ Efficiency\ (\%) = \frac{PTX\ in\ crude\ mixture - unloaded\ PTX}{PTX\ in\ crude\ mixture} \times 100\% \quad (1)$$

To determine the loading of PTX SPNPs, the PTX used was tagged with FITC. The high-pressure homogenization and EHD jetting procedures were conducted as described in previous sections. The collection and processing of the SPNPs were also performed as previously described. Standards were produced by dissolving a known weight of FITC-PTX in 9:1 ultrapure distilled water:methanol (v/v) from a range of 9.5 to 650 µg mL^{-1}. The standards contained the same amount of HSA that was in the SPNP composition. The SPNPs were resuspended in a water/methanol solvent system of that of the standards. Spectral readings of absorbance were read from 400 to 700 nm overnight. Absorbance values were recorded at 490 nm (λ_{max}). The NTA device was used as previously described to determine the size distribution of the FITC labeled PTX SPNPs in suspension. The following equation was used to calculate the loading efficiency.

$$Loading\ (\%) = \frac{m_{FITC-PTX,\ measured}}{V_{sample,\ SPNPs} * \rho_{SPNPs,hydrated} * \frac{m_{FITC-PTX,theoretical}}{m_{SPNPs,\ theoretical}}} \times 100\% \quad (2)$$

Where $m_{FITC-PTX,\ measured}$ represents the mass of FITC labeled PTX in the sample based on the absorbance measurements. $V_{sample,\ SPNPs}$ denotes the accumulated volume of all FITC labeled PTX SPNPs in the sample and is calculated using NTA size distribution. $\rho_{SPNPs,hydrated}$ represents the density of the hydrated SPNPs and was calculated through multiplying the density of the dry particles by the swelling ratio. $\frac{m_{FITC-PTX,theoretical}}{m_{SPNPs,\ theoretical}}$ represents the theoretical mass fraction of FITC-PTX with respect to the total mass of FITC labeled PTX SPNPs and was determined from the composition of the homogenized FITC-PTX-HSA solution.

OL61 and NPD Cell Survival Assay: Mouse OL61 (shp53/NRAS/EGFRvIII) and NPD-AC2 (shp53/NRAS/PDGFß) cells were plated at a density of 1000 cells per well in a 96-well cell culture plate 24 h before treatment. Cells were then incubated with either Abraxane or with PTX-HSA for 72 h in triplicate wells per condition to determine the half maximal inhibitory concentration (IC_{50}). After the IC_{50} doses were established, both cell types were treated with either HSA SPNPs, HSA-PTX, PTX (0.2 µM) or PTX SPNPs at their respective IC_{50} dosed for 72 h in triplicate wells per condition. Cell viability was determined with CellTiter-Glo 2.0 Luminescent Cell Viability Assay following the manufacturer's protocol. The resulting luminescence was read with the Enspire Multimodal Plate Reader (PerkinElmer, Model 2300-0000). Data were represented graphically using the GraphPad Prism software (version 8), and statistical significance was determined by one-way ANOVA followed by Tukey's test for multiple comparisons.

Tumor Implantation: Mice were anesthetized using ketamine (75 mg kg^{-1}, i.p) and dexmedetomidine (0.5 mg kg^{-1}, i.p) before stereotactic implantation with NPDAC2 (10K) cells in the right striatum. The coordinates for implantation were as follows: 0.5 mm anterior and 2.0 mm lateral from the bregma and 3.0 mm ventral from the dura. Neurospheres were injected at a rate of 1 µL min^{-1}. Mice were given a combination of buprenorphine (0.1 mg kg^{-1}) and carprofen (5 mg kg^{-1}) for analgesia.[37] One week post implantation, mice were randomly divided into the following groups: Saline, Irradiation (I.R.), Abraxane, Abraxane +IR, HSA SPNP, PTX SPNP, and PTX SPNP+IR. Upon reaching the symptomatic tumor stage, blood from these mice was collected to perform the serum chemistry, and further mice were perfused with tyrodes solution to collect the brain, liver, and spleen. All procedures involving mice were performed following policies set by the Association for Assessment and Accreditation of Laboratory Animal Care (AAALAC) and the Institutional Animal Care and Use Committee (IACUC) at the University of Michigan (PRO00011290).

In Vivo Radiation: The groups treated with radiation alone or combined with Abraxane or PTX SPNP were subjected to an irradiation (I.R.) dose of 2 Gy for 5 days/week for 2 weeks for a total of 20 Gy of ionizing radiation. Irradiation treatment was done as follows: Mice were gently anesthetized with isoflurane and positioned under a copper orthovoltage source. The irradiation beam was targeted toward the brain while protecting the body with iron collimators. Irradiation treatment was performed at the University of Michigan Radiation Oncology Core.[32,37]

Complete Blood Serum Biochemistry: Blood from the submandibular vein of tumor-bearing mice was taken and transferred to serum separation tubes (Biotang). Samples were left at room temperature for 60 min to allow blood coagulation in the serum separation tubes. The samples were centrifuged at 2000 rpm (400 × g) for 15 min. Complete serum chemistry for each sample was determined by in vivo animal core at the University of Michigan.

PTX SPNP In Vivo Dosing: In the in vivo dosing regimen, Abraxane was administered intravenously (I.V.) at 5 mg kg^{-1}. Concurrently, SPNPs were administered at 6.2 mg kg^{-1} (200 µL/mouse) through tail vein injections. Doses of Abraxane and SPNPs were administered every Monday, Wednesday, and Friday for two weeks. The total dose of PTX within the Abraxane was 0.50 mg kg^{-1} and was 0.58 mg kg^{-1} from the PTX SPNPs.

Immunohistochemistry: For neuropathological assessment of the brains, they were first fixed in 4% paraformaldehyde (PFA) and embedded in paraffin. Five micron thick sections were made using a microtome system (Leica RM2165). The sections were permeabilized with TBS-0.5% Triton-X (TBS-Tx) for 20 min, followed by antigen retrieval at 96 °C with 10 mM sodium citrate (pH 6) for 20 min. The sections were cooled to room temperature (R.T.), followed by washing five times with TBS-Tx (5 min per wash), and blocked with 5% goat serum in TBS-Tx for 1 h at R.T. Brain sections were incubated with primary antibody GFAP (1:200), MBP (1:200), CD68 (1:1000), Anti-Iba1 (1:2000) diluted in 1% goat serum TBS-Tx overnight at 4 °C. The next day, sections were washed with TBS-Tx five times and incubated with biotinylated secondary antibody diluted 1:1000 in 1% goat serum TBS-Tx in the dark for 4 h. Biotin-labeled sections were subjected to 3, 3′- diaminobenzidine (DAB) (Biocare Medical) with nickel sulfate precipitation. The reaction was quenched with 10% sodium azide; sections were washed three times in 0.1 M sodium acetate, followed by dehydration in xylene, and coverslipped with DePeX Mounting Medium (Electron Microscopy Sciences). Images were obtained using brightfield microscopy (Olympus BX53) at 10× and 40× magnification. Brain sections, with a thickness of 5 µm, were prepared from each experimental group. These sections were embedded in paraffin for subsequent analysis of tumor size. Following embedding, they underwent staining with hematoxylin and eosin (H&E).[29] In particular, sections encompassing the tumor were imaged using brightfield microscopy (Olympus BX53) setting. For histological assessment, livers were embedded in paraffin, sectioned 5 µm thick using the microtome system, and H&E stained. Brightfield images were obtained using the Olympus MA BX53 microscope.[29]

Statistical Analysis: Statistical analysis was performed using Prism 9.4.1 (GraphPad Software). Samples were first tested for normality prior to performing the statistical analysis method. A statistical threshold of $p = 0.05$ was used where p-values <0.05 were considered statistically significant. No experimental values were excluded from the analysis.

Supporting Information

Supporting Information is available from the Wiley Online Library or from the author.

Acknowledgements

This work had been supported by the National Institute of Health Grant R01-NS124167 and the "Center of Complex Particle Systems (COMPASS)" (Grant No. NSF 2243104). Ava Mauser acknowledges support from the National Science Foundation Graduate Research Fellowship under Grant No. DGE 1256260. The authors acknowledge the financial support of the University of Michigan College of Engineering and NSF grant #DMR-0320740, and technical support from the Michigan Center for Materials Characterization. In addition, the authors acknowledge the financial support of the University of Michigan and the Biointerfaces Institute for use of the instruments and technical assistance. The authors would also like to acknowledge the University of Michigan Biomedical Research Core Facilities Microscopy Core.

Conflict of Interest

The authors declare no conflict of interest.

Data Availability Statement

The data that support the findings of this study are available from the corresponding author upon reasonable request.

Keywords

Abraxane, cancer, glioblastoma, nanoparticles, paclitaxel

Received: May 15, 2024
Published online:

[1] E. D. Zanders, F. Svensson, D. S. Bailey, *Drug Discov. Today* **2019**, *24*, 1193.
[2] L. P. Ganipineni, F. Danhier, V. Préat, *J. Control. release Off. J. Control. Release Soc.* **2018**, *281*, 42.
[3] A. O. Awosika, M. C. Farrar, T. F. Jacobs, in *Treasure Island (FL)*, StatPearls **2019**.
[4] S. B. Horwitz, *Trends Pharmacol. Sci.* **1992**, *13*, 134.
[5] M. A. Foote, *Biotechnol. Annu. Rev.* **2007**, *13*, 345.
[6] B. R. B. Weiss, R. C. Donehower, P. H. Wiernik, T. Ohnuma, R. J. Gralla, D. L. Trump, J. R. Baker, D. A. Van Echo, D. D. Von Hoff, B. Leyland-jones, *J. Clin. Oncol.* **1990**, *8*, 1263.
[7] H. Gelderblom, J. Verweij, K. Nooter, A. Sparreboom, *Eur. J. Cancer* **2001**, *37*, 1590.
[8] L. Van Zuylen, M. O. Karlsson, J. Verweij, E. Brouwer, P. De Bruijn, K. Nooter, G. Stoter, A. Sparreboom, *Cancer Chemother. Pharmacol.* **2001**, *47*, 309.
[9] P. Ma, R. J. Mumper, *J. Nanomed. Nanotechnol.* **2013**, *4*, 1000164.
[10] D. A. Yardley, *J. Controlled Release* **2013**, *170*, 365.
[11] A. M. Sofias, M. Dunne, G. Storm, C. Allen, *Adv. Drug Delivery Rev.* **2017**, *122*, 20.
[12] D. Y. Zhang, C. Dmello, L. Chen, V. A. Arrieta, E. Gonzalez-Buendia, J. R. Kane, L. P. Magnusson, A. Baran, C. D. James, C. Horbinski, A. Carpentier, C. Desseaux, M. Canney, M. Muzzio, R. Stupp, A. M. Sonabend, *Clin. Cancer Res. Off. J. Am. Assoc. Cancer Res.* **2020**, *26*, 477.
[13] N. Habibi, A. Mauser, Y. Ko, J. Lahann, *Adv. Sci.* **2022**, *9*, 2104012.
[14] J. V. Gregory, P. Kadiyala, R. Doherty, M. Cadena, S. Habeel, E. Ruoslahti, P. R. Lowenstein, M. G. Castro, J. Lahann, *Nat. Commun.* **2020**, *11*, 1.
[15] M. S. Alghamri, K. Banerjee, A. A. Mujeeb, A. Mauser, A. Taher, R. Thalla, B. L. McClellan, M. L. Varela, S. M. Stamatovic, G. Martinez-Revollar, A. V. Andjelkovic, J. V. Gregory, P. Kadiyala, A. Calinescu, J. A. Jiménez, A. A. Apfelbaum, E. R. Lawlor, S. Carney, A. Comba, S. M. Faisal, M. Barissi, M. B. Edwards, H. Appelman, Y. Sun, J. Gan, R. Ackermann, A. Schwendeman, M. Candolfi, M. R. Olin, J. Lahann, et al., *ACS Nano* **2022**, *16*, 8729.
[16] D. Furtado, M. Björnmalm, S. Ayton, A. I. Bush, K. Kempe, F. Caruso, *Adv. Mater.* **2018**, *30*, 46.
[17] A. Pawar, S. Thakkar, M. Misra, *J. Controlled Release* **2018**, *286*, 179.
[18] N. P. Desai, C. Tao, L. Louie, P. Shoon-Shiong, *Formulations of Pharmacological Agents, Methods for the Preparation Thereof and Methods for the Use Thereof*, United States patent US 8137684B2 **2012**.
[19] S. K. Boda, X. Li, J. Xie, *J. Aerosol Sci.* **2018**, *125*, 164.
[20] N. J. Greenfield, *Nat. Protoc.* **2006**, *1*, 2876.
[21] A. Mauser, D. F. Quevedo, B. Zhang, Y. Hernandez, A. Berardi, W. Brown, S. Lee, R. Miki, J. Raymond, J. Lahann, C. F. Greineder, *Adv. Ther.* **2023**, *6*, 2300007.
[22] A. A. Salem, M. Lotfy, A. Amin, M. A. Ghattas, *Biochem. Biophys. Rep.* **2019**, *20*, 100670.
[23] S. Siddiqui, F. Ameen, S. ur Rehman, T. Sarwar, M. Tabish, *J. Mol. Liq.* **2021**, *336*, 116200.
[24] S. L. Richheimer, D. M. Tinnermeier, D. W. Timmons, *Anal. Chem.* **1992**, *64*, 2323.
[25] R. H. Abbassi, A. Recasens, D. C. Indurthi, T. G. Johns, B. W. Stringer, B. W. Day, L. Munoz, *ACS Pharmacol. Transl. Sci.* **2019**, *2*, 402.
[26] S. Masoumi, A. Harisankar, A. Gracias, F. Bachinger, T. Fufa, G. Chandrasekar, F. Gaunitz, J. Walfridsson, S. S. Kitambi, *Drug Des. Devel. Ther.* **2016**, *10*, 2881.
[27] A. L. Risinger, F. J. Giles, S. L. Mooberry, *Cancer Treat. Rev.* **2009**, *35*, 255.
[28] A.-A. Calinescu, F. J. Núñez, C. Koschmann, B. L. Kolb, P. R. Lowenstein, M. G. Castro, *J. Vis. Exp.* **2015**, *96*, 52443.
[29] A.-A. Calinescu, V. N. Yadav, E. Carballo, P. Kadiyala, D. Tran, D. B. Zamler, R. Doherty, M. Srikanth, P. R. Lowenstein, M. G. Castro, *Clin. Cancer Res.* **2017**, *23*, 1250.
[30] A. Comba, P. J. Dunn, A. E. Argento, P. Kadiyala, M. Ventosa, P. Patel, D. B. Zamler, F. J. Núñez, L. Zhao, M. G. Castro, P. R. Lowenstein, *Neuro. Oncol.* **2020**, *22*, 806.
[31] C. Koschmann, A.-A. Calinescu, F. J. Nunez, A. Mackay, J. Fazal-Salom, D. Thomas, F. Mendez, N. Kamran, M. Dzaman, L. Mulpuri, J. Krasinkiewicz, R. Doherty, R. Lemons, J. A. Brosnan-Cashman, Y. Li, S. Roh, L. Zhao, H. Appelman, D. Ferguson, V. Gorbunova, A. Meeker, C. Jones, P. R. Lowenstein, M. G. Castro, *Sci. Transl. Med.* **2016**, *8*, 328ra28.
[32] F. J. Núñez, F. M. Mendez, P. Kadiyala, M. S. Alghamri, M. G. Savelieff, M. B. Garcia-Fabiani, S. Haase, C. Koschmann, A.-A. Calinescu, N. Kamran, M. Saxena, R. Patel, S. Carney, M. Z. Guo, M. Edwards, M. Ljungman, T. Qin, M. A. Sartor, R. Tagett, S. Venneti, J. Brosnan-Cashman, A. Meeker, V. Gorbunova, L. Zhao, D. M. Kremer, L. Zhang, C. A. Lyssiotis, L. Jones, C. J. Herting, J. L. Ross, et al., *Sci. Transl. Med.* **2019**, *11*, eaaq1427.
[33] N. Habibi, A. Mauser, J. E. Raymond, J. Lahann, *Beilstein J. Nanotechnol.* **2022**, *13*, 274.
[34] A. J. Miles, S. G. Ramalli, B. A. Wallace, *Protein Sci.* **2022**, *31*, 37.
[35] L. Whitmore, B. A. Wallace, *Nucleic Acids Res.* **2004**, *32*, W668.
[36] L. Whitmore, B. A. Wallace, *Biopolymers* **2008**, *89*, 392.
[37] P. Kadiyala, S. V. Carney, J. C. Gauss, M. B. Garcia-Fabiani, S. Haase, M. S. Alghamri, F. J. Núñez, Y. Liu, M. Yu, A. Taher, F. M. Nunez, D. Li, M. B. Edwards, C. G. Kleer, H. Appelman, Y. Sun, L. Zhao, J. J. Moon, A. Schwendeman, P. R. Lowenstein, M. G. Castro, *J. Clin. Invest.* **2021**, *131*, 4.